Effects of hybridization on pelvic morphology: A macaque model

Laura T. Buck[a,b,*], David C. Katz[b, c], Rebecca Rogers Ackermann[d, e], Leslea J. Hlusko[f,g], Sree Kanthaswamy[h], Timothy D. Weaver[b]

[a] School of Biological and Environmental Sciences, Liverpool John Moores University, UK

[b] Department of Anthropology, University of California Davis, USA

[c] University of Calgary Cumming School of Medicine, Canada

[d] Department of Archaeology, University of Cape Town, South Africa

[e] Human Evolution Research Institute, University of Cape Town, South Africa

[f] Department of Integrative Biology, University of California Berkeley, USA

[g] Centro Nacional de Investigación sobre la Evolución Humana (CENIEH), Burgos, Spain

[h] School of Natural and Mathematical Sciences, Arizona State University, USA

Corresponding author.

Email address: l.buck@ljmu.ac.uk (L.T. Buck)

Effects of hybridization on pelvic morphology: A macaque model

Abstract

Ancient DNA analyses have shown that interbreeding between hominin taxa occurred multiple times. Though admixture is often reflected in skeletal phenotype, the relationship between the two remains poorly understood, hampering interpretation of the hominin fossil record. Direct study of this relationship is often impossible due to the paucity of hominin fossils and difficulties retrieving ancient genetic material. Here, we use a sample of known-ancestry hybrids between two closely related nonhuman primate taxa (Indian and Chinese *Macaca mulatta*) to investigate the effect of admixture on skeletal morphology. We focus on pelvic shape, which has potential fitness implications in hybrids, as mismatches between maternal pelvic and fetal cranial morphology are often fatal to mother and offspring. As the pelvis is also one of the skeletal regions that differs most between *Homo sapiens* and Neanderthals, investigating the pelvic consequences of interbreeding could be informative regarding the viability of their hybrids. We find the effect of admixture in *M. mulatta* is small and proportional to the relatively small morphological difference between the parent taxa. Sexual dimorphism appears to be the main determinant of pelvic shape in *M. mulatta*. The lack of difference in pelvic shape between Chinese and Indian *M. mulatta* is in contrast to that between Neanderthals and *H. sapiens,* despite a similar split time (in generations) between the hybridizing pairs. Greater phenotypic divergence between hominins may relate to adaptations to disparate environments, but may also highlight how the unique degree of cultural buffering in hominins allowed for greater neutral divergence. In contrast to some previous work identifying extreme morphologies in first- and second-generation hybrids, here the relationship between pelvic shape and admixture is linear. This linearity may be because most sampled animals have a multi-generational admixture history or because of relatively high constraints on the pelvis compared to other skeletal regions.

Keywords:

Hybridization; Human evolution; Primate; Skeletal morphology; Geometric morphometric methods; *Macaca mulatta*

1. Introduction

Elucidating the effects of hybridization is critical for understanding the context of human evolution and the processes driving it (Ackermann et al., 2016). The past few years have seen great methodological advances in ancient DNA (aDNA) analyses, enabling the detection of interbreeding events and resulting in an increased appreciation of their frequency and importance (for reviews see Gopalan et al., 2021; Wolf and Akey, 2018). Despite these advances, we are still far from understanding the importance of gene flow between hominin lineages in determining morphology and from recognising hybrids in the fossil record (Warren et al., 2018). Claims of hybrid Neanderthal/*Homo sapiens* fossils were made for decades before supporting genetic evidence was available (Duarte et al., 1999; Trinkaus et al., 2003a, 2003b; Rougier et al., 2007). When the data are limited to fossil material and its archaeological context, however, these assertions are almost inevitably subject to counter-claims, such as those asserting that intermediate morphology is within the boundaries of intraspecific variation in *H. sapiens* (e.g., Tattersall and Schwartz, 1999).

In many cases, even now, preservation issues mean there is limited potential for aDNA evidence to resolve the question of which putative (morphological) hybrids are actual (genetic) hybrids. There have nonetheless been some spectacular finds. One such was the aDNA analysis of the Oase 1 mandible from Romania, which showed that this *H. sapiens* individual did indeed have a recent Neanderthal ancestor (Fu et al., 2015), as had been suggested from its morphology (Trinkaus et al., 2003a; 2003b; Rougier et al., 2007). Though the exact relationship between Oase 1's hybrid ancestry and suggested Neanderthal traits is not clear, the fact that it was identified as a hybrid based on both morphology and genetics supports a growing body of research indicating that signatures of hybridization are detectable in skeletal morphology.

Here we build on existing research using nonhuman primates to inform our understanding of hominin hybrids (e.g., Ackermann et al., 2006, 2014; Boel et al., 2019; Martinez et al., 2019). We use a large sample of captive full-bred and admixed Chinese and Indian rhesus macaques (*Macaca mulatta*) to elucidate the expected morphological consequences of admixture between closely related primate species, including hominins. Of particular interest because Chinese and Indian *M. mulatta* have been mixing in this captive colony for decades, the study also examines how admixture effects on phenotype vary with ancestry contributions from the two subspecies lines.

1.1. The effects of hybridization on the pelvis

We focus on the effects of hybridization on pelvic morphology. In some primates, these effects may be particularly acute due to interactions between the functional and physiological constraints of locomotion and parturition (Trevathan, 2015; Kawada et al., 2020). The pelvis is also a

region of divergent shape in *H. sapiens* and *H. neanderthalensis* (Rak and Arensburg, 1987; Weaver and Hublin, 2009). Combined with neonatal crania that, although less distinct than the adult crania of these taxa, are also differently shaped (Ponce de León and Zollikofer, 2001; Gunz et al., 2012), this could have had implications for the viability of hybrid offspring. A more Neanderthal-like fetal cranium and a more *H. sapiens*-like birth canal could have led to increased likelihood of dystocia and the potential death of both mother and child. These severe consequences would have constituted a strong selective pressure likely to shape morphology, as has been suggested for the effect of caesarean sections on fetopelvic disproportion in recent humans (Mitteroecker et al., 2016, 2017). To the best of our knowledge, the relationship between pelvic morphology and admixture in the fossil record has not yet been addressed, most likely due to the paucity of both suitable well-preserved fossils and postcranial material from extant known hybrids. Thus, it is a skeletal region from which we might learn a considerable amount, regarding the morphological impact of hybridization, by adopting an approach based on nonhuman primate analogues.

1.1. Macaca mulatta *taxonomy*

The genus *Macaca* is divided into four species groups. The *fascicularis* group, which contains *M. mulatta,* is the most widely distributed (Fooden, 1976, 2006). In 2000, Fooden reported that *M. mulatta* inhabited Southeast and South Asia with a geographic range of ~15–36 N° and ~70–120 °E, although this range was historically wider and has likely been further reduced in the last two decades. Fossils show that *M. mulatta*, or a very similar precursor, was present in its current range by >40 ka, notwithstanding the last glacial maximum, which likely caused local extinctions and subsequent post-glacial in-migrations in some presently inhabited regions (Fooden, 2000).

There is substantial disagreement over the systematics of *M. mulatta*, which appears to be polyphyletic: mitochondrial DNA (mtDNA) analyses cluster Chinese *M. mulatta* with *M. cyclopis* or *M. fuscata*, rather with than their supposed conspecifics, including Indian *M. mulatta* (Melnick et al., 1993; Hayasaka et al., 1996). MtDNA also suggests deep divergences between geographic groups of *M. mulatta* to at least subspecific level, although there remains disagreement as to how many subspecies should be recognised (Zhang and Shi, 1993; Smith and Mcdonough, 2005). Indeed, the divergence between Indian and Chinese *M. mulatta* mtDNA is deeper than between some well-accepted species pairs of macaques such as *M. assamensis* and *M. thibetana* (Hayasaka et al., 1996; Smith and Mcdonough, 2005). Similar divisions between Chinese and Indian *M. mulatta* have also been found in studies of protein polymorphisms, microsatellite single nucleotide polymorphisms (SNPs), and MHC alleles (Smith and Mcdonough, 2005; Ferguson et al., 2007).

Here we refer to Chinese and Indian *M. mulatta* as different subspecies solely to avoid more confusing terms, such as 'group' or 'population'. Our analyses are not intended to address the validity or otherwise, of that taxonomic designation. The differences between extant Chinese and Indian *M. mulatta* subspecies, particularly the molecular and physiological differences, have been studied extensively due to the species' role as a biomedical model. Chinese-derived *M. mulatta* have greater genetic heterozygosity (Smith and Mcdonough, 2005; Ferguson et al., 2007; Kanthaswamy et al., 2009) and morphological diversity (Fooden, 2000) than Indian-derived animals. Indeed, Smith and McDonough (2005) found pairwise differences between Indian *M. mulatta* populations to be half as great as between comparable pairs of human populations, despite the extremely low levels of genetic variation in *H. sapiens* (Smith and Mcdonough, 2005). These low levels of variation may be due to a bottleneck experienced by Indian populations in their recent evolutionary past (Smith and Mcdonough, 2005; Hernandez et al., 2007; Kanthaswamy et al., 2009). Because Neanderthals also appear to have had small population sizes and low genetic diversity (Green et al., 2010; Bocquet-Appel and Degioanni, 2013), this is another way in which this *M. mulatta* cross-sample is an interesting analogue for hybridization during human evolution.

Relative to the known genetic differences, the extent of morphological variation within *M. mulatta* and between Chinese and Indian groups is less clear. Fooden (e.g., 1976, 1982, 1995, 2000, 2006) argues that although there is substantial geographic variation in phenotype, the pattern of variation within *M. mulatta* is insufficiently clear to warrant subspecific divisions (Fooden, 2000). Fooden's (1995, 2000) taxonomy is based on a conservative designation requiring at least one trait with discontinuous variation between groups. Many other researchers, however, have noted substantial morphological differences between Indian- and Chinese-derived animals in particular (see discussion in Fooden, 2000). For example, Chinese males are larger than Indian males, which may reflect adaptation to a colder climate, following Bergmann's rule (Bergmann, 1847; Clarke and O'Neil, 1999). Indeed, across the species' natural range, stature and mass tend to increase gradually with latitude, although there are regional exceptions to this trend (Fooden, 2000). Tail length decreases with longitude, particularly east of 95 °E, and is, therefore, longer in Indian than in Chinese *M. mulatta* (Fooden, 2000; Hamada et al., 2005). In captive-bred Chinese and Indian *M. mulatta* housed in Louisiana, USA (Tulane National Primate Research Center), there are differences in patterns of sexual dimorphism, with greater sexual dimorphism in Chinese than Indian monkeys (Clarke and O'Neil, 1999). These studies suggest that size, allometric shape, and patterns of sexual dimorphism may be variables that differ between the two *M. mulatta* taxa and which therefore may vary in admixed individuals.

Chinese and Indian *M. mulatta* have been isolated from one another since at least the Late Pleistocene (Zhang and Shi, 1993; Smith and Mcdonough, 2005), likely since ~162 ka, based on genetic analyses of ~1,500 SNPs (Hernandez et al., 2007). Given a generation time of approximately 7.5 years (Wolfe, 1986) and the split time of ~162 ka (Hernandez et al., 2007), about 21,600 generations passed between the divergence of Indian and Chinese *M. mulatta* and their interbreeding in the California National Primate Research Center (CNPRC) colony in the mid-1980s (see sub-section 2.1). The same calculation for *H. sapiens* and Neanderthals depends upon more assumptions and disputed dates, but an approximate estimation of the same variables is possible. If we use a relatively conservative split date of 550–765 ka (Meyer et al., 2016), a generation length of 26–30 years (Moorjani et al., 2016), and a date for interbreeding of 47–65 ka (Sankararaman et al., 2012), the middle point of each range results in a rough estimate of 21,482 generations between divergence and interbreeding. The macaque and hominin taxa can thus be argued to have had similar degrees of divergence between taxon pairs at the time of introgression, making the *M. mulatta* an interesting model for examining Neanderthal/*H. sapiens* hybridization.

1.2. Hybridization in nonhuman primates

Hybridization appears to be commonplace in the primate order, occurring in all major lineages (Cortés-Ortiz et al., 2019). Some well-established macaque species, such as *M. arctoides*, are even thought to have hybrid origins (Tosi et al., 2000). Ackermann and colleagues (e.g., Ackermann et al., 2006, 2014, 2019; Ackermann and Bishop, 2010) have used nonhuman primates as hominin analogues to study the potential effects of hybridization during human evolution. The majority of this work has been carried out on baboons, which are well studied, provide a good ecological analogue for hominins (Jolly, 2001; for review see Fischer et al., 2019), and are housed in several major captive colonies with known pedigree information. Ackermann et al. (2006, 2014) showed that first- and second-generation olive x yellow baboon hybrids exhibit extreme size (heterosis) and size variation outside the parental ranges. They also display high frequencies of unusual non-metric cranial traits, dental and sutural anomalies. This body of work, supported by other research on nonhuman primate hybridization (for reviews, see Ackermann et al., 2019; Cortés-Ortiz et al., 2019), provides some important insights to underpin the current study. Notably, there is a skeletal signal of hybridization and the effects of hybridization appear to be similar across primate taxa, albeit with an effect of phylogenetic proximity, such that more extreme hybrids are more likely to result from interbreeding between more divergent taxa. It also provides some expectations to test with our macaque data: that hybrid primates generally show increased variation and heterosis compared to parent taxa.

2. Materials and methods

2.1. Sample

Our sample is composed of *M. mulatta* housed at the CNPRC, University of California Davis. The CNPRC colony was initially composed entirely of Indian *M. mulatta*, but following a ban on exporting primates from India in 1978, the colony's managers introduced a small number of Chinese animals to maintain genetic variation within the population. The first interbreeding was recorded in 1983 (Kanthaswamy et al., 2009). Unlike many nonhuman hybrid studies, which focus on the first few hybrid generations (e.g., Ackermann et al., 2006, 2014; Savriama et al., 2018; Warren et al., 2018), interbreeding between Indian and Chinese *M. mulatta* has been occurring in this colony for at least four to five generations (based on a generation time of ~7.5 years; Wolfe, 1986). The colony now provides a sample with a distribution from full-bred Indian to full-bred Chinese animals, including many individuals with low percentages of Chinese ancestry. This range of admixture is a better representation of what we might expect in natural hybrid zones and in the hominin fossil record if hybridization leads to viable offspring (Kelaita and Cortés-Ortiz, 2013; Fuzessy et al., 2014). In effect, the Indian *M. mulatta* housed at the CNPRC are a population experiencing a relatively small amount of genetic input from another taxon (Chinese *M. mulatta*); this can be seen as analogous to a Pleistocene *H. sapiens* population undergoing a small number of time-limited interbreeding events with Neanderthals.

Our sample data consisted of 138 full-body medical computed tomography (CT) scans from adult (>6 years) *M. mulatta* housed at the CNPRC: 94 females and 44 males. Sex ratios in the CNPRC colony are deliberately kept unbalanced to reduce intramale fighting, resulting in unequal numbers of available males and females. To optimize the spread of admixture proportions (Chinese ancestry) in our sample we included more females than males; however, we sought to maintain the same degree of female bias in both Indian and Chinese *M. mulatta* samples to the extent possible. We included 19 full-bred Indian *M. mulatta*, 17 full-bred Chinese *M. mulatta*, and hybrid animals with a range of admixture proportions (Table 1). Estimates of Chinese ancestry were obtained from the CNPRC and are constructed from pedigree records. In our aim to obtain the best range of admixture in our sample, we included individuals with some arthritis if the original morphology was sufficiently unobscured as to allow confident landmark placement (see below); however, we removed six animals with pathological pelves from our initial sample after examination of their CT scans, leaving the final sample of 138 (Table 1).

All animals were CT scanned at the CNPRC by appropriately trained staff. CT-scanning and all other experimental procedures for this study were approved by the Institutional Animal Care and Use

Committee at the University of California, Davis (protocol #19057). In most cases, monkeys were sedated and scanned in vivo. Although in a few cases monkeys were scanned as cadavers, no monkeys were sacrificed for this study. As they become available, macerated skeletal remains from cadavers of animals involved in this study are being curated in the Department of Anthropology, University of California Davis. CT scans from the sample are also freely available on request via the MorphoSource digital archive (Morphosource.org; project name: The Rhesus Macaque Admixture Project).

[Table 1 placement]

2.2. Data collection

Using the CT scans, in Avizo v. 9.1 Lite (ThermoFisher Scientific, Waltham, MA, USA) we virtually segmented the skeleton from the other tissue types and the pelvis from the rest of the skeleton using a mixture of automatic and manual thresholding and segmentation tools. To collect landmark coordinates for analyses using geometric morphometric methods (GMM), we digitized landmarks and semilandmarks on virtual reconstructions using Avizo (shaded isosurfaces and transparent volume renderings) and exported the coordinates for analysis in R v. 3.5.2–3.6.3 (R Core Team, 2018). We collected 48 true landmarks plus semilandmarks describing seven curves by digitizing many points along each curve (Fig. 1; Table 2). These curve semilandmarks then were resampled in R using a custom script, so that each curve contained the same number of semilandmarks for each individual, as follows: curve 1 (40 semilandmarks), curves 2 and 3 (18 semilandmarks each), curves 4 and 5 (30 landmarks each), and curves 6 and 7 (10 landmarks each). After processing, our data set consisted of 204 total landmarks: 48 true landmarks and 156 semilandmarks. We selected landmarks and semilandmarks with the intent to optimally characterize the size and shape of the pelvis. We examined intraobserver error by using ten repetitions each of two individuals digitized repeatedly, with more than a day elapsing between each digitizing session. We processed each landmark configuration as described below and compared the Procrustes distances between iterations of the same individual vs. those between different individuals (see Results).

[Figures 1 and 2 and Table 2 placement]

2.3. Methods of analysis

All analyses were carried out in R V. 3.5.2–3.6.3 (R Core Team, 2018) using the geomorph (Collyer and Adams, 2018, 2020; Adams et al., 2020) and Morpho (Schlager, 2017) packages and base R functions. To register the shape data we used the procSym function in Morpho (Schlager, 2017) to perform a generalized Procrustes superimposition of the landmarks, to slide the semilandmarks along their curves using a criterion of minimizing bending energy, and project the superimposed configurations into a tangent space. We performed principal components analysis (PCA) in geomorph (using the plotTangentSpace function) to summarize the high dimensional data into axes of greatest explanatory power and to visualize variation within and between groups of interest on these axes. We then used geomorph's procD.lm function to perform Procrustes analysis of variance (ANOVA) to test for relationships between predictor and response variables of interest and to compare model fits. To test for the presence of different patterns of sexual dimorphism in different admixture groups, we compared the fit of additive (shape ~ admixture + sex) and interactive (shape ~ admixture * sex) models of shape, sex, and admixture. This was to determine whether there were different patterns of sexual dimorphism in the different admixture groups. We also included a three-knot B spline model of admixture and sex-adjusted shape in the comparison to investigate whether departures from a linear relationship between sex and ancestry could result from genetic factors such as dominance or epistasis. The B-spline model allows for the relationship between the response and predictor variables to be described by a smooth curve.

Due to sexual dimorphism in our sample (described in more detail below), we used least squares linear regression to account for the effects of sex on admixture and shape. Because sex ratios varied with Chinese ancestry percentages, it was necessary to adjust both variables to control for the effect of sex entirely. The sex-adjusted residuals were used in all subsequent analyses of the relationship between shape and admixture.

To quantify and visualize the relationship between admixture and pelvic shape, we regressed pelvic shape on admixture using least squares linear regression and then projected the sex-adjusted shape observations onto the resulting regression vector to compute admixture scores (Drake and Klingenberg, 2008; Ledevin and Koyabu, 2019; Sheratt et al., 2019; Moore, 2021). Displayed in a bivariate plot, the results provide a straightforward way to compare the magnitude of shape differences attributable to admixture (the regression trend) to the magnitude of shape differences not explained by the model (residuals about the trend). To visualize the relative contributions of sex and admixture variables to overall shape variation, we display distributions of pairwise Procrustes distances between specimens using different filters of group and sex membership. To test for differences in variance we used the function morphol.disparity in geomorph (Adams et al., 2020; Collyer and Adams, 2020), which calculates the Procrustes variance for each group, the pairwise

distances between group variances and the *p*-values of tests of significant difference between pairs ($p < 0.05$ throughout).

3. Results

In our intraobserver error analysis, the mean Procrustes distances between iterations of the same individual were much smaller than those between different individuals and the 95% confidence intervals (CIs) of their means did not overlap. The mean Procrustes distance between iterations of the same individual were 0.026 (95% C.I.: 0.023–0.029) and 0.036 (95% C.I.: 0.024–0.048); between different individuals the mean Procrustes distance was 0.105 (95% C.I.: 0.101–0.109). We judged this to mean that levels of intraobserver error in our data were within acceptable limits.

As expected, given the known sexual dimorphism in macaque species (e.g., Plavcan, 2001) and the obstetric function of the pelvis, our initial Procrustes ANOVAs showed a relatively high degree of sexual dimorphism in the pelvic morphology of the complete sample: sex explains ~18% of the variation in shape ($F [1, 136] = 30.13$, $r^2 = 0.18$, $p < 0.05$). To investigate the nature of sexual dimorphism within the sample, we compared the fit of additive and interaction models of sex and shape (Table 3). The interaction model of the relationship between sex, admixture (% Chinese ancestry), and shape does not fit the data significantly better than a simple additive model, suggesting that sexual dimorphism does not vary with degree of admixture. This being the case, we used additive regression models with sex as the predictor and shape or admixture as the response, to produce residuals that allowed us to adjust for sex in both shape and admixture variables, for use in further analyses. These residuals are used in all subsequent analyses performed on the complete sample.

[Table 3 placement]

After adjusting for sex in both shape and admixture variables, the amount of Chinese ancestry explains a very small, though significant, portion of remaining shape variation: approximately 2% ($F [1, 136] = 3.07$, $r^2 = 0.02$, $p < 0.05$). The weak effect of admixture on shape, in contrast to sexual dimorphism, can be seen when pairwise Procrustes distances between the sexes in each Chinese ancestry category are compared to within-sex variation between categories (Fig. 3). Also shown in Figure 3 is variation between members of the same sex within the same admixture category. This can be considered baseline interindividual variation resulting from a combination of many factors, likely including age, weight, and lifetime experiences in the colony. Levels of variation between those with different Chinese ancestry categories, whether adjacent or more distant, are indistinguishable from

that baseline variation, demonstrating the very weak effect of admixture compared to other sources of interindividual variation.

[Figure 3 placement]

The effect of ancestry on pelvic shape (adjusting both for sex) is mostly evident in the shape of the iliac blades (Fig. 4). In animals with more Chinese ancestry the cranial border of the iliac blades is of relatively equal height, ventral to dorsal, whereas in animals with less Chinese ancestry, the iliac blades extend further laterally and the cranial edges are more angled, extending further cranially at their ventral extent. The dorsal part of the iliac blades, in the region of the vertebrae S2 and S3 (Fig. 1), also extends more caudally in animals with higher regression scores. There are further differences in the ischium: in higher-scoring animals, the medial border of the ischial tuberosities is more laterally placed, compared to animals with lower scores, and the superior border of the pubic symphysis is more ventrally placed. Finally, the sacrum differs between individuals which vary in regression score: higher-scoring individuals have a sacrum that is craniocaudally shorter and more ventrally orientated in the region of S2/S3. All of these differences are very slight, however.

[Figure 4 placement]

The relationship between regression scores and admixture displayed in Figure 4 appears to approach a linear or additive relationship, meaning that change in shape and increasing Chinese ancestry is relatively proportional. This is supported by model comparison, which shows that a three-knot B spline model does not fit the data significantly better than a simple linear model of shape and Chinese ancestry % (adjusted for sex; Table 4).

[Table 4 placement]

In the complete sample, there is no significant difference in pelvic centroid size between any pairwise group comparison of full-bred Indian, Chinese, or admixed groups (Table 5). Similarly, there are no significant differences between group variances, showing that no one group is more variable in pelvic shape than another (Table 6 and 7). This suggests there are no transgressive sizes and no increase in shape variation in admixed individuals in this sample.

[Tables 5, 6 and 7 placement]

3.1. Full-bred macaques

In contrast to the full sample analysis (Table 3), analysis of solely the Indian and Chinese full-breds indicates that an interaction model of the relationship between sex and shape is a significantly better fit for the data than an additive model (Table 8). This suggests a difference in sexual dimorphism between the two subspecies that is masked by the greater variation in the complete sample (see also Clarke and O'Neil, 1999). Due to these apparent differences in sexual dimorphism, in the full-bred sample we adjusted for differences in the effects of sex on shape separately for each subspecies, by adding the difference between the subspecies-specific male and female means to the female configurations for each subspecies. A PCA showing the separation between the subspecies on the main axes of sex-adjusted shape can be seen in Figure 5. The sex-adjusted residual shapes were used as response variables in a Procrustes ANOVA to quantify the effect of subspecies designation on shape ($F [1, 34] = 1.47$, $r^2 = 0.07$, $p < 0.05$). After accounting for sexual dimorphism, there is a significant but fairly weak relationship between the remaining shape variation and subspecies designation (Fig. 6). Designation as Indian or Chinese subspecies accounts for approximately 7% of pelvic shape variation in the full-bred sample.

[Tables 8 and Figures 5 and 6 placement]

Figure 6 shows the relationship between regression scores summarizing the proportion of sex-adjusted shape associated with subspecies designation, and subspecies designation itself. As with the full sample, there is a difference in pelvic shape associated with Chinese ancestry. Chinese individuals generally have higher regression scores than Indian individuals, showing that they inhabit a different region of the shape space. Compared to the Chinese mean shape, the Indian mean shape is characterized by dorsoventrally and mediolaterally broader iliac blades, which are more angled across the top, running from high ventrally to low dorsally, whereas the tops of the mean Chinese iliac blades are more level. The mean Indian sacrum is more dorsocaudally placed between the ilia and the sacral alae are shorter craniocaudally. The acetabulae of the mean Indian shape are placed more ventrolaterally and the pubic symphysis of the mean Indian shape is more dorsally orientated. Finally, the ischial tuberosities of the mean Indian shape extend more caudomedially than those of the mean Chinese shape. These shape differences echo what are seen in Figure 4 and suggest that more Chinese ancestry leads to a pelvis that more closely approaches the mean Chinese shape.

3.2. Projecting admixed individuals onto a vector of full-bred shape

The effect of admixture on sex-adjusted pelvic shape in the complete sample is small, as emphasized by the comparison with baseline inter-individual variation within a sex and ancestry category (Fig. 3). Our analyses show, however, that there is a significant relationship between Chinese ancestry and shape and suggest that this is relationship is broadly additive. To examine this possibility further, we created a vector of shape variation using only the sex-adjusted full-bred Indian and Chinese individuals (*n* = 36) and projected the sex-adjusted admixed individuals (*n* = 102) onto this vector (Fig. 7). This figure shows an idealized, linear relationship between Chinese ancestry and sex-adjusted pelvic shape. Comparison of Figures 4 and 7 shows there is very little difference between the modeled relationship and that obtained with the actual data, supporting the assertion that the proportion of Chinese ancestry affects pelvic shape in a predictable, proportional manner.

[Figure 7 placement]

4. Discussion

The effect of admixture on pelvic shape variation in Indian and Chinese *M. mulatta* is very slight. To put this into context, shape variation between individuals from different Chinese ancestry categories is no greater than intra-category (within sex) variation (Fig. 3). The latter shape variation probably results from multiple variables including age, weight, and stochastic variation. This is in clear contrast to the strong effect of sex on pelvic shape, which cuts across all Chinese ancestry categories.

4.1. The skeletal context

The low levels of pelvic shape differentiation between members of different Chinese ancestry categories are not surprising, given the relatively small differences we found between the full-bred subspecies (Fig. 5). Given the research discussed above (see Introduction) suggesting there are noticeable gross phenotypic differences between Indian and Chinese *M. mulatta* (Clarke and O'Neil, 1999; Fooden, 2000; Hamada et al., 2005), it is possible that the similarity we see in the pelvic data is particular to that region. Skeletal regions display different degrees of canalization and variation (Buck et al., 2010) and the strong selective pressures resulting from the requirements of parturition and locomotion might be expected to lead to stabilizing selection acting on the pelvis. The macaque fit between fetus and birth canal is relatively tight during birth, comparable with that seen in extant humans, and there is evidence in *M. mulatta* of selection on the pelvis to reduce cephalopelvic dystocia (Kawada et al., 2020). The current study is the first analysis of hybrid pelvic morphology. In fact, to the best of our knowledge, it is the first study of any postcranial shape in known hybrids

where skeletal shape has been analyzed directly, rather than through the use of proxy measurements taken by palpating bones through soft tissue in live animals (e.g., Kelaita and Cortés-Ortiz, 2013; Fuzessy et al., 2014). Thus, the effects of admixture more widely in human and nonhuman primate pelvic shape remain unknown, and the possibility of regional anatomical differences in admixture signature will be examined in forthcoming work on the crania and other bones from the same sample. If the phenotypic similarity between Chinese and Indian *M. mulatta* is replicated in other regions of the skeleton, these taxa may be relatively phenotypically undifferentiated (skeletally), despite clear genetic differences between them (Zhang and Shi, 1993; Smith and Mcdonough, 2005; Ferguson et al., 2007; Hernandez et al., 2007; Kanthaswamy et al., 2009).

4.2. The macaque context

Morphological research on hybrids between Japanese (*M. fuscata*), and Taiwanese (*M. cyclopis*) macaques shows results comparable to those presented here (Hamada et al., 2012; Ito et al., 2015; Boel et al., 2019). In particular, hybridization between *M. fuscata* and *M. cyclopis* results in a linear correspondence between relative tail length and degree of admixture, with no extreme phenotypes recorded (Hamada et al., 2012), contrary to what is seen for many other nonhuman primate hybrids (see below). *M. fuscata* and *M. cycopis* are estimated to have a divergence time of ~170 ka (Chu et al., 2007), close to the ~162 ka estimated for Indian and Chinese *M. mulatta* (Hernandez et al., 2007). GMM-based cranial analyses of these hybrids show no greater levels of variation in hybrids than in parent species and no clear effects of hybrid status on the frequency of anomalous nonmetric traits (Boel et al., 2019). Qualitative comparison of PCAs of the morphospace inhabited by the two full-bred samples, however, does seem to indicate a greater degree of separation between *M. fuscata* and *M. cyclopis* than between the *M. mulatta* subspecies, and a tendency of all hybrids towards *M. fuscata* shape, rather than the linear relationship with admixture we describe for our sample (Boel et al., 2019; see also analysis of linear measurements in Ito et al., 2015). The Japanese x Taiwanese hybrids were wild-caught in Japan (Ito et al., 2015; Boel et al., 2019), at a higher latitude and in a more temperate climate than Taiwan. Therefore, there may be some adaptive advantage in *M. fuscata* morphology leading to the dominance of *M. fuscata*-like morphology in hybrids and also potentially selection for greater phenotypic divergence between the parent taxa after their separation in the Pleistocene, if their habitats are less similar than those of Indian and Chinese *M. mulatta*.

4.3. The nonhuman primate context

In contrast to much of the previous research on nonhuman primates (Ackermann et al., 2006, 2014; Kelaita and Cortés-Ortiz, 2013; Fuzessy et al., 2014) with the exception of other macaque studies (see above), in this study we found no increased shape variation and no heterosis or transgressive size in the hybrid sample. There are several possible factors that may contribute to this difference from earlier work, including the methods used, the range of admixture of the hybrids making up each sample, the skeletal regions studied, and the degree of similarity (phenotypic or genetic) between the parent taxa in each study.

In the current study we used landmark-based GMM to compare overall pelvic shape, while by contrast, most studies of hybrid morphology in nonhuman primates (e.g., Ackermann et al., 2006, 2014; Kelaita and Cortés-Ortiz, 2013; Fuzessy et al., 2014; Ito et al., 2015) have used traditional morphometrics and nonmetric traits. This may, in part, account for differences in results between studies, as analysis of individual nonmetric traits or measurements can emphasize greater difference in specific regions that may be averaged out by GMM analyses of overall shape. Similar GMM used to analyze shape in hybrid mouse crania show patterns of increased variation and extreme phenotypes similar to those seen in baboons (Warren et al., 2018), however, suggesting that GMM are not entirely responsible for the differences in results between studies.

Hybridization in the baboon colony studied by Ackermann and colleagues (2006, 2014) was only a few generations deep and many transgressive or anomalous morphologies characterized as the products of hybridization are most likely to occur in the F1 generation or in generations close to the interbreeding event (Prentis et al., 2008). This likely contributes to our lack of such a signal in the current sample, which contains fewer early generation hybrids and only one F1 individual. More subtle manifestations of expected hybrid morphology, however, such as some individuals of transgressive size/shape and greater variation within admixed samples, have also been documented in naturally hybridizing populations of marmosets and howler monkeys, where far fewer individuals are likely to be early generation hybrids (Kelaita and Cortés-Ortiz, 2013; Fuzessy et al., 2014). This suggests that the admixture proportions sampled here may not completely explain the more linear relationship between admixture and pelvic morphology in our results.

A final possible reason for the novelty of our results, in relation to the majority of nonhuman hybrid research, may be relatively short divergence time between the *M. mulatta* parent taxa compared to the parent taxa investigated in previous work. Baboon taxonomy is much debated, but a recent paper by Rogers et al. (2019) suggests the lineages of the olive and yellow baboon allotaxa studied by Ackermann and colleagues (Ackermann et al., 2006, 2014) diverged about 1.4 Ma. Black (*Alouatta pigra*) and mantled (*A. palliata*) howler monkeys, as studied by Kelaita et al. (2013), are still more phylogenetically divergent, with a split time of ~3 Ma (Kelaita and Cortés-Ortiz, 2003), whilst

Callithrix is a fairly young genus and the black-tufted and white-headed marmosets (*C. penicillata* and *C. geoffroyi*, respectively), whose hybrids have been studied by Fuzessy and colleagues (2014), split ~700 ka (Malukiewicz et al., 2017). Based on these dates, the genetic distance between Indian and Chinese *M. mulatta*, estimated to have diverged ~162 ka (Hernandez et al., 2007), is considerably less than between these other taxa. There also remains the possibility that the rhesus macaques are less differentiated morphologically relative to their genetic distance, perhaps due to stabilizing selection (see also sub-section 4.4 below). This is an interesting possibility, which has not yet been investigated and which should be followed up by the comparison of further nonhuman primate taxa pairs with similar phylogenetic divergence times.

The differences between results presented here and previous work on nonhuman primate hybrids, as well as between previous studies, demonstrate the complex relationship between taxonomic divergence and hybrid morphology, which is not yet fully understood. Likewise, these differences indicate the need for further investigation to better understand which nonhuman primate species make the best models for hominin hybridization. It has been shown that more genetically divergent taxa lead to more transgressive hybrids, due to increasing fixation of different alleles in each parent taxon over time (i.e., fixed differences in alleles as opposed to differences in allele frequencies), which may lead to complementary gene action or epistasis in hybrid offspring (Stelkens and Seehausen, 2009; Stelkens et al., 2009; Comeault and Matute, 2018; Allen et al., 2020). The relationship between phenotypic divergence and transgressive phenotypes is less clear, however (Stelkens and Seehausen, 2009; Stelkens et al., 2009), and relationships among divergence time, genetic and phenotypic differentiation appear to differ between groups of organisms (Stelkens and Seehausen, 2009; McGee et al., 2016). Most vertebrate research on these relationships to date has been in fish (Stelkens and Seehausen, 2009; Stelkens et al., 2009; McGee et al., 2016). Thus, it is also unclear how well these results translate to primates, making this area ripe for further investigation.

4.4. The paleoanthropological context

From a paleoanthropological point of view, it is relevant that there appears to be considerably less variation in pelvic shape between Indian and Chinese *M. mulatta* than between Neanderthals and *H. sapiens*, a hybridizing taxon pair with reasonably comparable levels of genetic relatedness (see Introduction). Further examination of other aspects of the *M. mulatta* skeleton and other pairs of nonhuman primate taxa will be required to determine whether, given their genetic distance, Indian and Chinese rhesus macaques are relatively phenotypically similar or whether *H. sapiens* and Neanderthals are more divergent than would be expected within the context of the Primate order. If shown to be present throughout the skeleton, low levels of phenotypic differentiation between

Chinese and Indian *M. mulatta* might suggest stabilizing selection, whilst the mechanism leading to relatively high differentiation between the hominin taxa could be either directional selection or neutral evolution. If stabilizing selection has played a lesser role in the evolutionary history of the hominin pelvis than that of macaques, this could reflect a wider trend. For example, Schroeder and von Cramon Taubadel (2017) have shown that across all sampled extant hominoid taxa, hominoid cranial evolution is characterized by stabilizing selection with very few exceptions, one of which is marked directional selection in the hominin lineage after its split with the chimpanzee lineage. The pelvic evidence from the current study may suggest that this pattern holds throughout the skeleton. The presence of unusually high levels of phenotypic differentiation in hominins (Lynch, 1990) is supported by comparison of rates of cranial evolution in the *Pan* clade versus the Neanderthal/*H. sapiens* clade (Weaver, 2014) and by comparisons between Neanderthal/*H. sapiens* morphological divergence and that between other catarrhine pairs (Harvati et al., 2004). It has been suggested that a unique human ecological niche, typified by cultural adaptation, has allowed the build-up of uncommonly great neutral variation in our lineage due to reduced selection (including stabilizing selection) compared to other organisms (Ackermann and Cheverud, 2004; Wells and Stock, 2007; Weaver and Stringer, 2015; Buck et al., 2019).

There is, however, also a strong argument for selection leading to greater pelvic variation between *H. sapiens* and Neanderthals than between Indian and Chinese *M. mulatta*. Indian and Chinese-derived *M. mulatta* are likely phenotypically similar, at least in part because they have inhabited similar habitats since their divergence (Hamada et al., 2005). This is in contrast to *H. sapiens* and Neanderthals, which adapted for hundreds of thousands of years to the disparate climates and habitats of Africa and Western Eurasia, respectively (Holliday, 1997a, b). Climate has played a role in extant human pelvic shape variation (Betti et al., 2014), and it is also thought to have affected pelvic morphology in extinct hominins (Ruff, 1993; Weaver, 2009). In addition to, or as an alternative to the effects of climate, directional selection leading to cranial vault expansion in the hominin lineage, as reported by Schroeder and von Cramon Taubadel (2017), could play a role in pelvic change via the requirement for congruence during parturition. If this is the case, the simultaneous cranial expansion but divergent cranial shapes in the *H. sapiens* and Neanderthal lineages could have contributed to their differences in pelvic morphology.

The seeds of relatively great divergence in pelvic shape between hominin species may lie still deeper in hominin evolution. It has been suggested that integration has been relaxed in the human pelvis relative to other hominids, allowing for greater evolvability and selection for bipedal morphology (Grabowski et al., 2011). This possibility is borne out by the high levels of intraspecific geographic variation in human pelvic morphology compared to other skeletal regions (Betti and

Manica, 2018). A breakdown in integration is likely governed by changes to the underlying genetic architecture controlling pelvic development, and evidence that distinctive hominin pelvis shape results from a unique growth trajectory emerging relatively early in development also suggests modification of genetically determined pathways (Zirkle and Lovejoy, 2019). Different genetic underpinning and levels of integration in macaques and hominins could mean that similar degrees of genetic difference could affect phenotypic outcomes in different ways. This scenario could facilitate the potential development of adaptive differences in one group (e.g., Neanderthals/*H. sapiens*), but neutral divergence in the other (e.g., Indian/Chinese *M. mulatta*). We note that the possibilities of directional selection and unusually high neutral variation are not mutually exclusive and could have combined to produce particularly phenotypically divergent taxa in *H. sapiens* and Neanderthals.

One could argue that, due to their lower levels of phenotypic disparity relative to the time depth of their divergence, Indian/Chinese *M. mulatta* pelves are not a good model for the phenotypic effects of hybridization in hominins. It may, however, be difficult to find a pair of primate taxa with a similar divergence time to *H. sapiens*/Neanderthals and similar morphological disparity, highlighting the peculiarity of these hominin sister taxa. Most of the taxon pairs in the nonhuman primate hybrid literature have greater phylogenetic split times and, although there is no way of directly comparing parent taxon phenotypic disparity between studies, the stronger admixture effects seen in previous studies may in part be related to greater phenotypic differentiation between parent taxa (see sub-section 4.3).

Although weak, the linear nature of the relationship between admixture and pelvic shape we find here is nonetheless informative. Greater Chinese ancestry leads to a pelvic shape which is closer to the mean shape for full-bred Chinese individuals, and the difference in Chinese ancestry is proportional to the difference in pelvic shape. If further investigation bears out the suggestion of the results we present here—that the morphology of hybrids between closely related primate taxa is proportional to the input of each parent taxon—this information can be used to further investigate the expected morphology of hominin hybrids. Models of expected hominin hybrid morphology can be constructed with the known morphology of parent taxa; for example, Neanderthal and *H. sapiens* crania as the endpoints of the hypothetical shape vector along which all admixed individuals would fall. Thus, the magnitude of disparity between parental shapes would not affect the pattern of the hybrids that fall between them, if the pattern of variation is a valid analogue.

5. Conclusions

From a large sample of multigenerational hybrids and full-bred Indian and Chinese *M. mulatta*, we find the effects of admixture on pelvic shape to be very small, albeit significant, comparable with interindividual differences between members of the same sex and admixture category. The admixture signal we identify is linear, with greater Chinese ancestry resulting in a pelvic shape that more closely approximates that of full-bred Chinese *M. mulatta*. We find no evidence for an increase in size or shape variation, nor transgressive morphologies in hybrids. Taken in the context of the existing nonhuman primate hybrid literature, the small effect and additive nature of the admixture signal in *M. mulatta* pelvic shape is likely affected by a combination of factors, including the phylogenetic closeness of the parent taxa relative to that between previously studied taxon pairs (Ackermann et al., 2006, 2014; Kelaita and Cortés-Ortiz, 2013; Fuzessy et al., 2014), the similarity of Indian and Chinese *M. mulatta* habitat and ecological niche since their divergence (Hamada et al., 2005), and the low number of early generation hybrids in the current study. Despite the interesting disparity in phenotypic divergence between the Indian and Chinese *M. mulatta* and Neanderthals/*H. sapiens*, which deserves further investigation, the relative similarity in phylogenetic closeness (see also Allen et al., 2020) and the multiple generations of hybridization in the current sample of *M. mulatta*, have resulted in a useful analogue for hominin hybridization. Models of hypothetical outcomes of hybridization between Neanderthals and *H. sapiens*, using the pattern revealed by these *M. mulatta* results, can now be tested against the fossil record to increase our understanding of the impacts of interbreeding on human evolution.

Acknowledgments

This research was funded by the National Science Foundation (BCS 1623366, 1720128) and the Leakey Foundation. We thank the Editor, Associate Editor and three anonymous reviewers for their constructive comments, which have much improved this article. We thank Mark Grote for his substantial statistical assistance and CNPRC staff, including Alice Tarantel for overseeing CT scanning, and Paul-Michael Sosa, Daniel Quiros Molina, Jennifer Short, and Sarah Davis for their extensive help with data collection. We thank Irene Englis and staff at the University of California Davis Museum of Fish and Wildlife Biology for skeletonising remains involved in this study. LTB is grateful to Alex Cantó Pastor, Austin Reynolds, Mark Grabowski, Aurélien Mounier and Florent Détroit for help with coding, and we thank Amber Parks and Sara Jhanjar for all their help with segmenting CT scans.

607

608 References

609 Ackermann, R.R., Arnold, M.L., Baiz, M.D., Cahill, J.A., Cortés-Ortiz, L., Evans, B.J., Grant, B.R., Grant,
610 P.R., Hallgrimsson, B., Humphreys, R.A., Jolly, C.J., Malukiewicz, J., Percival, C.J., Ritzman, T.B.,
611 Roos, C., Roseman, C.C., Schroeder, L., Smith, F.H., Warren, K.A., Wayne, R.K., Zinner, D., 2019.
612 Hybridization in human evolution: Insights from other organisms. Evol. Anthropol. 28, 189–209.
613 Ackermann, R.R., Bishop, J.M., 2010. Morphological and molecular evidence reveals recent
614 hybridization between gorilla taxa. Evolution 64, 271–290.
615 Ackermann, R.R., Cheverud, J.M., 2004. Detecting genetic drift versus selection in human evolution.
616 Proc. Natl. Acad. Sci. USA 101, 17946–17951.
617 Ackermann, R.R., Mackay, A., Arnold, M.L., 2016. The hybrid origin of "Modern" Humans. Evol. Biol.
618 43, 1–11.
619 Ackermann, R.R., Rogers, J., Cheverud, J.M., 2006. Identifying the morphological signatures of
620 hybridization in primate and human evolution. J. Hum. Evol. 51, 632–645.
621 Ackermann, R.R., Schroeder, L., Rogers, J., Cheverud, J.M., 2014. Further evidence for phenotypic
622 signatures of hybridization in descendent baboon populations. J. Hum. Evol. 76, 54–62.
623 Adams, D.C., Collyer, M.L., Kaliontzopoulou, A., 2020. Geomorph: Software for geometric
624 morphometric analyses. Ver. 3.2.1. https://cran.r-project.org/package=geomorph
625 Allen, R., Ryan, H., Davis, B.W., King, C., Frantz, L., Irving-pease, E., Barnett, R., Linderholm, A., Loog, L.,
626 Haile, J., Lebrasseur, O., White, M., Kitchener, A.C., Murphy, W.J., Larson, G., Murphy, W.J.,
627 2020. A mitochondrial genetic divergence proxy predicts the reproductive compatibility of
628 mammalian hybrids. Proc. Royal Soc. B. Biol. Sci. 287, 20200690.
629 Bergmann, C.A., 1847. Uber die verhaltnisee der warmeokonomie der thiere zu iher grosse. Gottingen
630 Studien 1, 595–708.
631 Betti, L., Manica, A., 2018. Human variation in the shape of the birth canal is significant and
632 geographically structured. Proc. Royal Soc. B. Biol. Sci. 285, 20181807.
633 Betti, L., von Cramon-Taubadel, N., Manica, A., Lycett, S.J., 2014. The interaction of neutral
634 evolutionary processes with climatically-driven adaptive changes in the 3D shape of the human
635 os coxae. J. Hum. Evol. 73, 64–74.
636 Bocquet-Appel, J.P., Degioanni, A., 2013. Neanderthal demographic estimates. Curr. Anthropol. 54,
637 S202–S213.
638 Boel, C., Curnoe, D., Hamada, Y., 2019. Craniofacial shape and nonmetric trait variation in hybrids of
639 the Japanese macaque (*Macaca fuscata*) and the Taiwanese macaque (*Macaca cyclopis*). Int. J.
640 Primatol. 40, 214–243.

641 Buck, L.T., De Groote, I., Hamada, Y., Hassett, B.R., Ito, T., Stock, J.T., 2019. Evidence of different
642 climatic adaptation strategies in humans and non-human primates. Sci. Rep. 9, 11025.
643 Buck, L.T., Stock, J.T., Foley, R. a., 2010. Levels of intraspecific variation within the catarrhine skeleton.
644 Int. J. Primatol. 31, 779–795.
645 Chu, J.H., Lin, Y.S., Wu, H.Y., 2007. Evolution and dispersal of three closely related macaque species,
646 *Macaca mulatta, M. cyclopis*, and *M. fuscata*, in the eastern Asia. Molec. Phylogenet. Evol. 43,
647 418–429.
648 Clarke, M.R., O'Neil, J.A.S., 1999. Morphometric comparison of Chinese-origin and Indian-derived
649 rhesus monkeys (*Macaca mulatta*), Am. J. Primatol. 74. 335-346
650 Collyer, M.L., Adams, D.C., 2018. RRPP: An R package for fitting linear models to high-dimensional
651 data using residual randomization. Methods Ecol. Evol. 9, 1772–1779.
652 Collyer, M.L., Adams, D.C., 2020. RRPP: Linear model evaluation with randomized residuals in a
653 permutation procedure. Ver. 0.5.2, https://cran.r-project.org/package=RRPP.
654 Comeault, A.A., Matute, D.R., 2018. Genetic divergence and the number of hybridizing species affect
655 the path to homoploid hybrid speciation. Proc. Natl. Acad. Sci. USA 115, 9761–9766.
656 Core Team, R., 2018. R: A language and environment for statistical computing. Ver. 3.6.3.
657 Cortés-Ortiz, L., Bermingham, E., Rico, C., Rodríguez-Luna, E., Sampaio, I., Ruiz-García, M., 2003.
658 Molecular systematics and biogeography of the Neotropical monkey genus, *Alouatta*. Molec.
659 Phylogenet. Evol. 26, 64–81.
660 Cortés-Ortiz, L., Roos, C., Zinner, D., 2019. Introduction to special issue on primate hybridization and
661 hybrid zones. Int. J. Primatol. 40, 1-8.
662 Drake, A.G., Klingenberg, C.P., 2008. The pace of morphological change: Historical transformation of
663 skull shape in St. Bernard dogs. Proc. Royal Soc. B. Biol. Sci. 275, 71–76.
664 Duarte, C., Maurício, J., Pettitt, P.B., Souto, P., Trinkaus, E., Van Plicht, H. Der, Zilhão, J., 1999. The
665 early Upper Paleolithic human skeleton from the Abrigo do Lagar Velho (Portugal) and modern
666 human emergence in Iberia. Proc. Natl. Acad. Sci. USA 96, 7604–7609.
667 Ferguson, B., Street, S.L., Wright, H., Pearson, C., Jia, Y., Thompson, S.L., Allibone, P., Dubay, C.J.,
668 Spindel, E., Norgren, R.B., 2007. Single nucleotide polymorphisms (SNPs) distinguish Indian-
669 origin and Chinese-origin rhesus macaques (*Macaca mulatta*). BMC Genomics. 8, 43.
670 Fischer, J., Higham, J.P., Alberts, S.C., Barrett, L., Beehner, J.C., Bergman, T.J., Carter, A.J., Collins, A.,
671 Elton, S., Fagot, J., Ferreira da Silva, M.J., Hammerschmidt, K., Henzi, P., Jolly, C.J., Knauf, S.,
672 Kopp, G.H., Rogers, J., Roos, C., Ross, C., Seyfarth, R.M., Silk, J., Snyder-Mackler, N., Staedele, V.,
673 Swedell, L., Wilson, M.L., Zinner, D., 2019. The natural history of model organisms: insights into
674 the evolution of social systems and species from baboon studies. eLife. 8, e50989.

675 Fooden, J., 1976. Provisional classification and key to living species of macaques (Primates: *Macaca*).
676 Folia Primatol. 25, 225–236.
677 Fooden, J., 1982. Ecogeographic segregation of macaque species. Primates 23, 574-579.
678 Fooden, J., 1995. Systematic review of Southeast Asian longtail macaques, *Macaca fascicularis*
679 (Raffles, 1821). Fieldiana Zool. 81, 2-3.
680 Fooden, J., 2000. Zoology systematic review of the rhesus macaque, *Macaca mulatta* (Zimmermann,
681 1780). Field Museum of Natural History, Chicago.
682 Fooden, J., 2006. Comparative review of fascicularis-group species of macaques (Primates: *Macaca*).
683 Fieldiana Zool. 107, 1-43.
684 Fu, Q., Hajdinjak, M., Moldovan, O.T., Constantin, S., Mallick, S., Skoglund, P., Patterson, N., Rohland,
685 N., Lazaridis, I., Nickel, B., Viola, B., Prüfer, K., Meyer, M., Kelso, J., Reich, D., Pääbo, S., 2015. An
686 early modern human from Romania with a recent Neanderthal ancestor. Nature 524, 216–219.
687 Fuzessy, L.F., Silva, I. de O., Malukiewicz, J., Silva, F.F.R., Pônzio, M. do C., Boere, V., Ackermann, R.R.,
688 2014. Morphological variation in wild marmosets (*Callithrix penicillata* and *C. geoffroyi*) and their
689 hybrids. Evol. Biol. 41, 480–493.
690 Gopalan, S., Atkinson, E.G., Buck, L.T., Weaver, T.D., Henn, B.M., 2021. Inferring archaic introgression
691 from hominin genetic data. Evol. Anthropol, 30, 199–220.
692 Grabowski, M.W., Polk, J.D., Roseman, C.C., 2011. Divergent patterns of integration and reduced
693 constraint in the human hip and the origins of bipedalism. Evolution 65, 1336–1356.
694 Green, R.E., Krause, J., Briggs, A.W., Maricic, T., Stenzel, U., Kircher, M., Patterson, N., Li, H., Zhai, W.,
695 Fritz, M.H.-Y., Hansen, N.F., Durand, E.Y., Malaspinas, A.-S., Jensen, J.D., Marques-Bonet, T.,
696 Alkan, C., Prüfer, K., Meyer, M., Burbano, H.A., Good, J.M., Schultz, R., Aximu-Petri, A., Butthof,
697 A., Höber, B., Höffner, B., Siegemund, M., Weihmann, A., Nusbaum, C., Lander, E.S., Russ, C.,
698 Novod, N., Affourtit, J., Egholm, M., Verna, C., Rudan, P., Brajkovic, D., Kucan, Z., Gusic, I.,
699 Doronichev, V.B., Golovanova, L. V, Lalueza-Fox, C., de la Rasilla, M., Fortea, J., Rosas, A.,
700 Schmitz, R.W., Johnson, P.L.F., Eichler, E.E., Falush, D., Birney, E., Mullikin, J.C., Slatkin, M.,
701 Nielsen, R., Kelso, J., Lachmann, M., Reich, D., Pääbo, S., 2010. A draft sequence of the
702 Neandertal genome. Science 328, 710–22.
703 Gunz, P., Neubauer, S., Golovanova, L., Doronichev, V., Maureille, B., Hublin, J.J., 2012. A uniquely
704 modern human pattern of endocranial development. Insights from a new cranial reconstruction
705 of the Neandertal newborn from Mezmaiskaya. J. Hum. Evol. 62, 300–313.
706 Hamada, Y., Watanabe, T., Chatani, K., Hayakawa, S., Iwamoto, M., 2005. Morphometrical comparison
707 between Indian- and Chinese-derived rhesus macaques (*Macaca mulatta*). Anthropol. Sci. 113,
708 183–188.

Hamada, Y., Yamamoto, A., Kunimatsu, Y., Tojima, S., Mouri, T., Kawamoto, Y., 2012. Variability of tail length in hybrids of the Japanese macaque (*Macaca fuscata*) and the Taiwanese macaque (*Macaca cyclopis*). Primates 53, 397–411.

Harvati, K., Frost, S.R., McNulty, K.P., 2004. Neanderthal taxonomy reconsidered: Implications of 3D primate models of intra- and interspecific differences. Proc. Natl. Acad. Sci. USA 101, 1147–52.

Hayasaka, K., Fujii, K., Horai, S., 1996. Molecular phylogeny of macaques: Implications of nucleotide sequences from an 896-base pair region of mitochondrial DNA. Mol. Biol. Evol. 13, 1044–1053.

Hernandez, R.D., Hubisz, M.J., Wheeler, D.A., Smith, D.G., Ferguson, B., Rogers, J., Nazareth, L., Indap, A., Bourquin, T., McPherson, J., Muzny, D., Gibbs, R., Nielsen, R., Bustamante, C.D., 2007. Demographic histories and patterns of linkage disequilibrium in Chinese and Indian rhesus macaques. Science 316, 240–243.

Holliday, T.W., 1997a. Postcranial evidence of cold adaptation in European Neandertals. Am. J. Phys. Anthropol. 104, 245–58.

Holliday, T.W., 1997b. Body proportions in Late Pleistocene Europe and modern human origins. J. Hum. Evol. 32, 423–448.

Ito, T., Kawamoto, Y., Hamada, Y., Nishimura, T.D., 2015. Maxillary sinus variation in hybrid macaques: implications for the genetic basis of craniofacial pneumatization. Biol. J. Linn. Soc. 115, 333–347.

Jolly, C.J., 2001. A proper study for mankind: Analogies from the papionin monkeys and their implications for human evolution. Am. J. Phys. Anthropol. 116, 177–204.

Kanthaswamy, S., Gill, L., Satkoski, J., Goyal, V., Malladi, V., Kou, A., Basuta, K., Sarkisyan, L., George, D., Smith, D.G., 2009. Development of a Chinese-Indian hybrid (Chindian) rhesus macaque colony at the California National Primate Research Center by introgression. J. Med. Primatol. 38, 86–96.

Kawada, M., Nakatsukasa, M., Nishimura, T., Kaneko, A., Morimoto, N., 2020. Covariation of fetal skull and maternal pelvis during the perinatal period in rhesus macaques and evolution of childbirth in primates. Proc. Natl. Acad. Sci. USA 117, 202002112.

Kelaita, M.A., Cortés-Ortiz, L., 2013. Morphological variation of genetically confirmed *Alouatta pigra* × *A. palliata* hybrids from a natural hybrid zone in Tabasco, Mexico. Am. J. Phys. Anthropol. 150, 223–234.

Ledevin, R., Koyabu, D., 2019. Patterns and constraints of craniofacial variation in colobine monkeys: Disentangling the effects of phylogeny, allometry and diet. Evol. Biol. 46, 14-34.

Lynch, M., 1990. The rate of morphological evolution in mammals from the standpoint of the neutral expectation. Am. Nat. 136, 727–741.

Malukiewicz, J., Hepp, C.M., Guschanski, K., Stone, A.C., 2017. Phylogeny of the *jacchus* group of

Callithrix marmosets based on complete mitochondrial genomes. Am. J. Phys. Anthropol. 162, 157–169.

Martinez, F.I., Capelli, C., Ferreira da Silva, M.J., Aldeias, V., Alemseged, Z., Archer, W., Bamford, M., Biro, D., Bobe, R., Braun, D.R., Habermann, J.M., Lüdecke, T., Madiquida, H., Mathe, J., Negash, E., Paulo, L.M., Pinto, M., Stalmans, M., Tátá, F., Carvalho, S., 2019. A missing piece of the *Papio* puzzle: Gorongosa baboon phenostructure and intrageneric relationships. J. Hum. Evol. 130, 1–20.

McGee, M.D., Neches, R.Y., Seehausen, O., 2016. Evaluating genomic divergence and parallelism in replicate ecomorphs from young and old cichlid adaptive radiations. Mol. Ecol. 25, 260–268.

Melnick, D.J., Hoelzer, G. a, Absher, R., Ashley, M. V, 1993. mtDNA diversity in rhesus monkeys reveals overestimates of divergence time and paraphyly with neighboring species. Mol. Biol. Evol. 10, 282–295.

Mitteroecker, P., Huttegger, S.M., Fischer, B., Pavlicev, M., 2016. Cliff-edge model of obstetric selection in humans. Proc. Natl. Acad. Sci. USA 113, 14680–14685.

Mitteroecker, P., Windhager, S., Pavlicev, M., 2017. Cliff-edge model predicts intergenerational predisposition to dystocia and Caesarean delivery. Proc. Natl. Acad. Sci. USA 114, 11669–11672.

Moore, A.J., 2021. Vertebral pneumaticity is correlated with serial variation in vertebral shape in storks. J. Anat. 238, 615-625.

Plavcan, J.M., 2001. Sexual dimorphism in primate evolution. Yearb. Phys. Anthropol. 44, 25-53.

Ponce de León, M.S., Zollikofer, C.P.E., 2001. Neanderthal cranial ontogeny and its implications for late hominid diversity. Nature 412, 534–538.

Prentis, P.J., Wilson, J.R.U., Dormontt, E.E., Richardson, D.M., Lowe, A.J., 2008. Adaptive evolution in invasive species. Trends Plant Sci. 13, 288–294.

Rak, Y., Arensburg, B., 1987. Kebara 2 Neanderthal pelvis: First look at a complete inlet. Am. J. Phys. Anthropol. 73, 227–231.

Rogers, J., Raveendran, M., Harris, R.A., Mailund, T., Leppälä, K., Athanasiadis, G., Schierup, M.H., Cheng, J., Munch, K., Walker, J.A., Konkel, M.K., Jordan, V.E., Steely, C.J., Beckstrom, T.O., Bergey, C., Burrell, A., Schrempf, D., Noll, A., Kothe, M., Kopp, G.H., Liu, Y., Murali, S., Billis, K., Martin, F.J., Muffato, M., Cox, L.A., Else, J., Disotell, T., Muzny, D.M., Phillips-Conroy, J., Aken, B., Eichler, E.E., Marques-Bonet, T., Kosiol, C., Batzer, M.A., Hahn, M.W., Tung, J., Zinner, D., Roos, C., Jolly, C.J., Gibbs, R.A., Worley, K.C., Archidiacono, N., Capozzi, O., Catacchio, C.R., Dinh, H.H., Doddapaneni, H.V., Han, Y., Huddleston, J., Jhangiani, S.N., Karimpour-Fard, A., Korchina, V., Kovar, C.L., Kuderna, L., Lee, S.L., Liu, X., Marra-Campanale, A., Mason, C.E., Montero, M. de M., Pagel, K.A., Palazzo, A., Pecotte, J., Pejaver, V., Pipes, L., Quick, V.S., Radivojac, P., Raja, A., Raney,

B.J., Rice, K., Rocchi, M., Sikela, J.M., Stanyon, R., Thomas, G.W.C., Ventura, M., Vilgalys, T.P., Vinar, T., Walter, L., 2019. The comparative genomics and complex population history of *Papio* baboons. Sci. Adv. 5, eaau6947.

Rougier, H., Milota, Ş., Rodrigo, R., Gherase, M., Sarcină, L., Moldovan, O., Zilhão, J., Constantin, S., Franciscus, R.G., Zollikofer, C.P.E., De León, M.P., Trinkaus, E., 2007. Peştera cu Oase 2 and the cranial morphology of early modern Europeans. Proc. Natl. Acad. Sci. USA 104, 1165–1170.

Ruff, C., 1993. Climatic adaptation and hominid evolution: The thermoregulatory imperative. Evol. Anthropol. 2, 53-60.

Savriama, Y., Valtonen, M., Kammonen, J.I., Rastas, P., Smolander, O.P., Lyyski, A., Häkkinen, T.J., Corfe, I.J., Gerber, S., Salazar-Ciudad, I., Paulin, L., Holm, L., Löytynoja, A., Auvinen, P., Jernvall, J., 2018. Bracketing phenogenotypic limits of mammalian hybridization. Roy. Soc. Open Sci. 5, 180903.

Schlager, S., 2017. Morpho and Rvcg - Shape analysis in R. In: Zheng, G., Li, S., Szekely, G. (Eds.), Statistical Shape and Deformation Analysis. Academic Press, Cambridge, pp. 217–256.

Schroeder, L., von Cramon-Taubadel, N., 2017. The evolution of hominoid cranial diversity: A quantitative genetic approach. Evolution 71, 2634–2649.

Sheratt, E., Sanders, K.L., Watson, A., Hutchinson, M.N., Lee, M.S. and Palci, A., 2019. Heterochronic shifts mediate ecomorphological convergence in skull shape of microcephalic sea snakes. Integr. Comp. Biol., 59, 616-624.

Smith, D.G., Mcdonough, J., 2005. Mitochondrial DNA variation in Chinese and Indian Rhesus macaques (*Macaca mulatta*). Am. J. Primatol. 65, 1–25.

Stelkens, R., Seehausen, O., 2009. Genetic distance between species predicts novel trait expression in their hybrids. Evolution 63, 884–897.

Stelkens, R.B., Schmid, C., Selz, O., Seehausen, O., 2009. Phenotypic novelty in experimental hybrids is predicted by the genetic distance between species of cichlid fish. BMC Evol. Biol. 9, 283.

Tattersall, I., Schwartz, J.H., 1999. Commentary hominids and hybrids: The place of Neanderthals in human evolution. Proc. Natl. Acad. Sci. USA 96, 7117-7119.

Tosi, A.J., Morales, J.C., Melnick, D.J., 2000. Comparison of Y chromosome and mtDNA phylogenies leads to unique inferences of macaque evolutionary history. Molec. Phylogenet. Evol. 17, 133–144.

Trevathan, W., 2015. Primate pelvic anatomy and implications for birth. Philos. Trans. Roy. Soc. B. Biol. Sci. 370, 20140065.

Trinkaus, E., 2003. Neandertal faces were not long; modern human faces are short. Proc. Natl. Acad. Sci. USA 100, 8142–8145.

811 Trinkaus, E., Milota, Ş., Rodrigo, R., Mircea, G., Moldovan, O., 2003a. Early modern human cranial
812 remains from the Peştera cu Oase, Romania. J. Hum. Evol. 45, 245–253.
813 Trinkaus, E., Moldovan, O., Milota, Ş., Bîlgăr, A., Sarcina, L., Athreya, S., Bailey, S.E., Rodrigo, R.,
814 Mircea, G., Higham, T., Bronk Ramsey, C., Van der Plicht, J., 2003b. An early modern human from
815 the Peştera cu Oase, Romania. Proc. Natl. Acad. Sci. USA 100, 11231–11236.
816 Warren, K.A., Ritzman, T.B., Humphreys, R.A., Percival, C.J., Hallgrímsson, B., Ackermann, R.R., 2018.
817 Craniomandibular form and body size variation of first generation mouse hybrids: A model for
818 hominin hybridization. J. Hum. Evol. 116, 57–74.
819 Weaver, T.D., 2009. The meaning of Neandertal skeletal morphology. Proc. Natl. Acad. Sci. USA 106,
820 16028-16033.
821 Weaver, T.D., 2014. Brief CoM. mulatta nication: Quantitative- and molecular-genetic differentiation
822 in humans and chimpanzees: Implications for the evolutionary processes underlying cranial
823 diversification. Am. J. Phys. Anthropol. 154, 615–620.
824 Weaver, T.D., Hublin, J., 2009. Neandertal birth canal shape and the evolution of human childbirth.
825 Proc. Natl. Acad. Sci. USA 106, 8151.
826 Weaver, T.D., Stringer, C.B., 2015. Unconstrained cranial evolution in Neandertals and modern
827 humans compared to common chimpanzees. Proc. Royal Soc. B. Biol Sci. 282, 20151519.
828 Wells, J.C.K., Stock, J.T., 2007. The biology of the colonizing ape. Am. J. Phys. Anthropol. 134, 191–
829 222.
830 Wolf, A.B., Akey, J.M., 2018. Outstanding questions in the study of archaic hominin admixture. PLoS
831 Genet. 14, e1007349.
832 Wolfe, L.D., 1986. Reproductive biology of rhesus and Japanese macaques. Primates 27, 95–101.
833 Zhang, Y.-P., Shi, L.-M., 1993. Phylogeny of rhesus monkeys (*Macaca mulatta*) as revealed by
834 mitochondrial DNA restriction enzyme analysis. Int. J. Primatol. 14, 587-605.
835 Zirkle, D., Lovejoy, C.O., 2019. The hominid ilium is shaped by a synapomorphic growth mechanism
836 that is unique within primates. Proc. Natl. Acad. Sci. USA 116, 13915–13920.
837

838 Figure legends

839

840 Figure 1. Landmarks and semilandmarks used in the analyses presented here viewed from (clockwise
841 from top left) ventral, cranial, caudal, dorsal, and right lateral views. Black spheres: true landmarks,
842 grey spheres: semilandmarks, lines: wireframe connecting landmarks and semilandmarks. For
843 landmarks that correspond to numbers, refer to Table 2. For ease of visualization, only true landmarks
844 are numbered, and they are numbered only in the view where they are most easily seen. In the
845 visualization of results throughout the remaining paper, only the wireframe is shown to better
846 visualize differences between shapes.

847

848 Figure 2. Semilandmark curves and wireframe used in the analyses presented here, viewed from (left
849 to right) anterior and posterior. 1: pelvic inlet (closed) curve, 2: right dorsal ischial curve, 3: left dorsal
850 ischial curve, 4: right iliac blade curve, 5: left iliac blade curve, 6: right pubic symphysis curve, 7: left
851 pubic symphysis curve.

852

853 Figure 3. Distributions of pairwise Procrustes distances generated directly from the data. Distributions
854 show distances between members of different sexes within a Chinese ancestry category (orange,
855 dashed line), between individuals of the same sex in the same Chinese ancestry category (grey, solid
856 line), in categories 12.5% apart/adjacent categories (turquoise, solid line), and in categories 50% apart
857 (purple, solid line). Variation between individuals in the same sex and ancestry category (grey, solid
858 line) may be considered baseline levels of variation against which to compare the effects of sex or
859 admixture.

860

861 Figure 4. Plot of regression scores showing the relationship between pelvic shape and admixture, both
862 adjusted for sex. Jitter is used to improve the visibility of separate points. Indian (0% Chinese
863 ancestry) in red, Chinese (100% Chinese ancestry) in dark blue, all other admixture percentages
864 shown as colour scale in between the two extremes, as shown to the right of the graph. Wireframes
865 below graph show minimum (in red) and maximum (in blue) scoring shapes on the regression score
866 axis with displacement magnified by two to aid visualization. Views shown (left to right) are ventral,
867 cranial, caudal, and right lateral.

868

869 Figure 5. PCA plot showing sex-adjusted shape differences between full-breds. PC1 accounts for
870 25.2% variance, PC2 accounts for 13.0% variance. Indian (0% Chinese ancestry) in red circles, Chinese

(100% Chinese ancestry) in dark blue squares. This PCA shows the large degree of overlap in pelvic shape between the subspecies on the primary axes of variation.

Figure 6. Regression score plot showing the relationship between sex-adjusted shape associated with subspecies designation and subspecies designation. Jitter is used to improve the visibility of separate points. Indian (0% Chinese ancestry) in red, Chinese (100% Chinese ancestry) in dark blue. Wireframes below graph show mean Indian shape (in red) and mean Chinese shape (in blue). Note that this differs from Figure 4, where the wireframes model the extremes of regression scores. As in Figure 4, displacement is magnified by two to aid visualization. Views shown (left to right) are ventral, cranial, caudal, and right lateral.

Figure 7. Regression score plot showing the relationship between sex-adjusted shape associated with Chinese ancestry and Chinese ancestry. Shapes of admixed individuals are projected on a vector constructed using fullbred shape only. Jitter is used to improve the visibility of separate points. Indian (0% Chinese ancestry) in red, Chinese (100% Chinese ancestry) in dark blue, all other admixture percentages shown as scale in between the two extremes, as shown to the right of the graph. Compare with Figure 4.

Figure 1

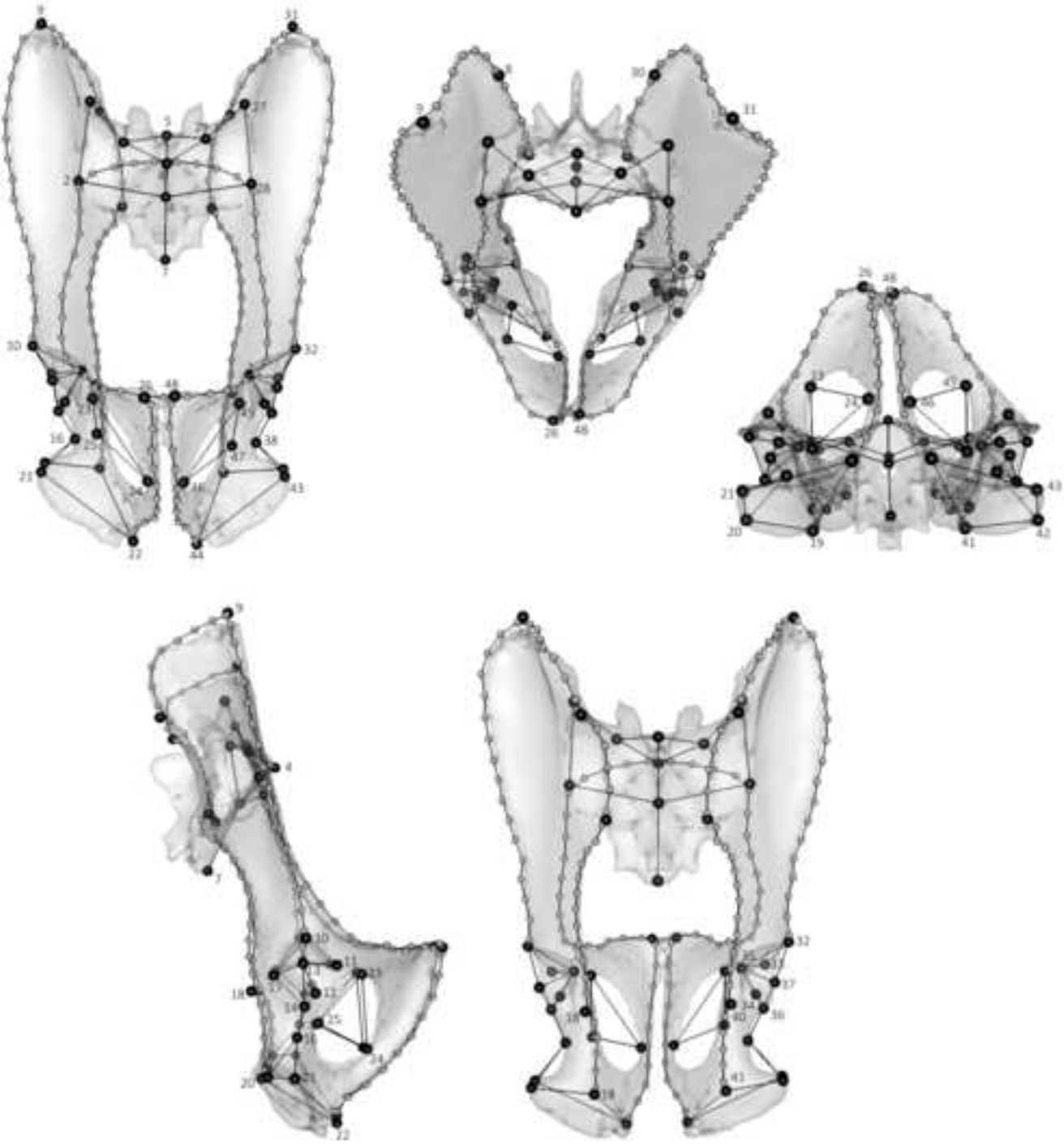

Figure 2

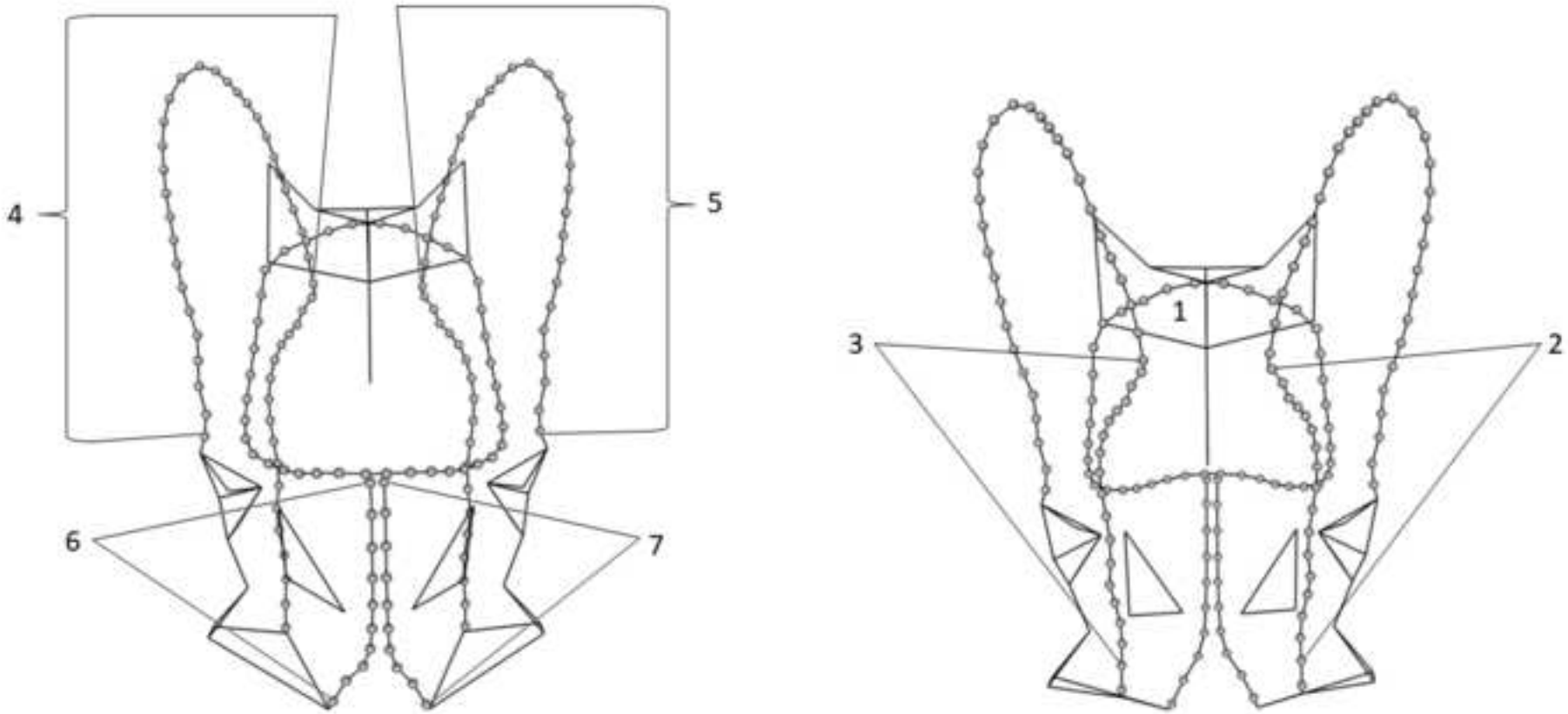

Figure 3

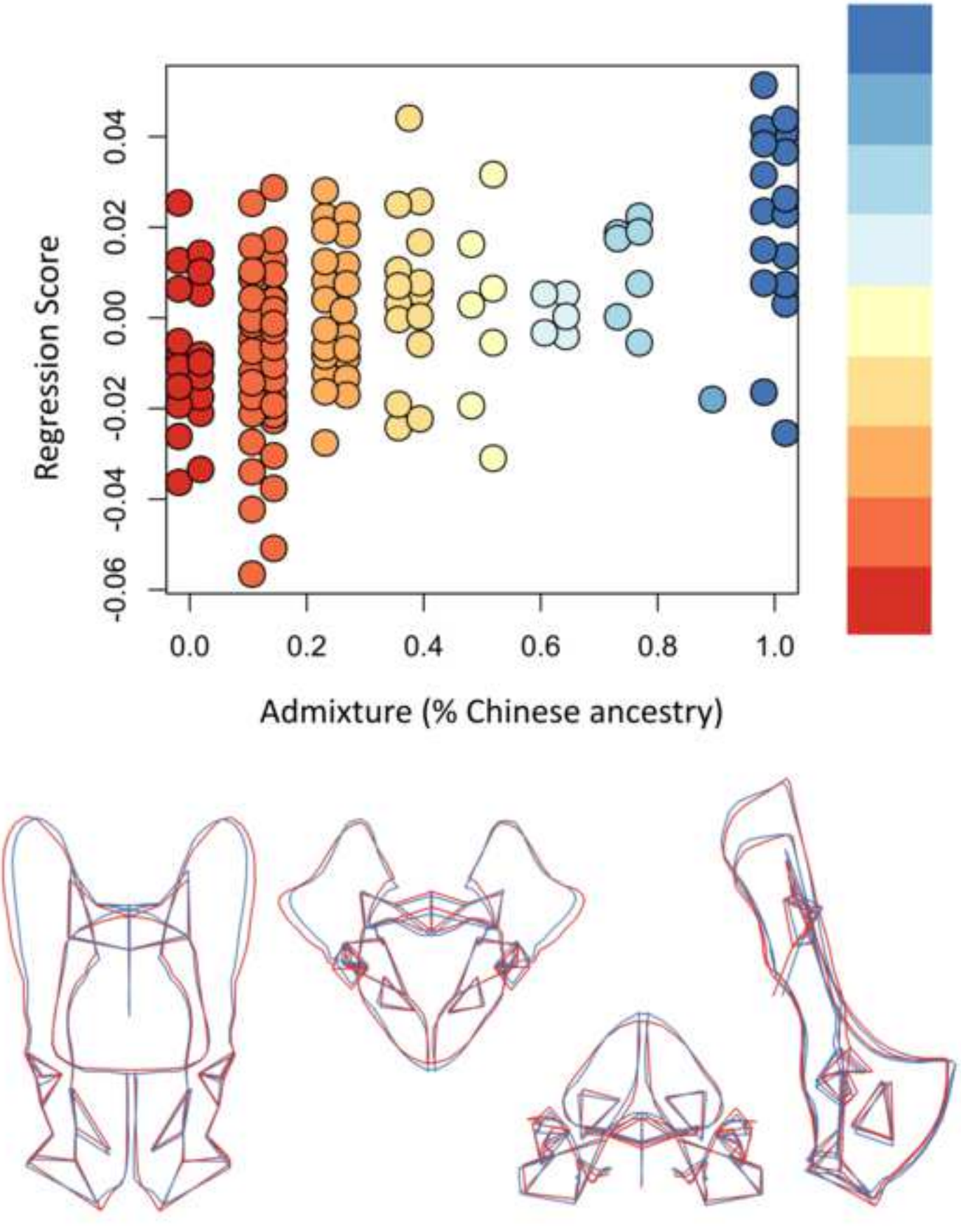
Regression Score
0.04
0.02
0.00
-0.02
-0.04
-0.06
0.0
0.2
0.4
0.6
0.8
1.0
Admixture (% Chinese ancestry)

Figure 4

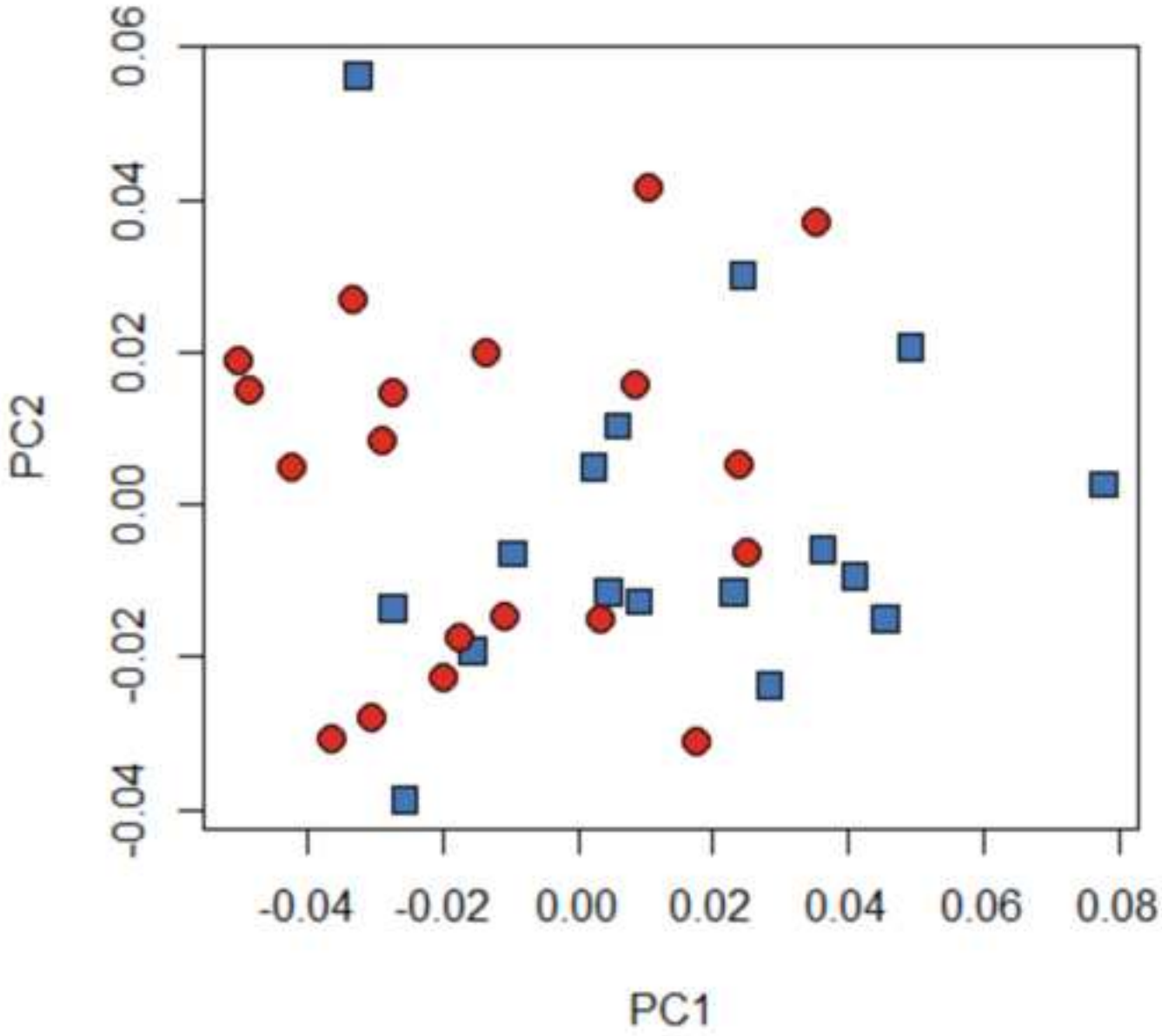

Figure 5

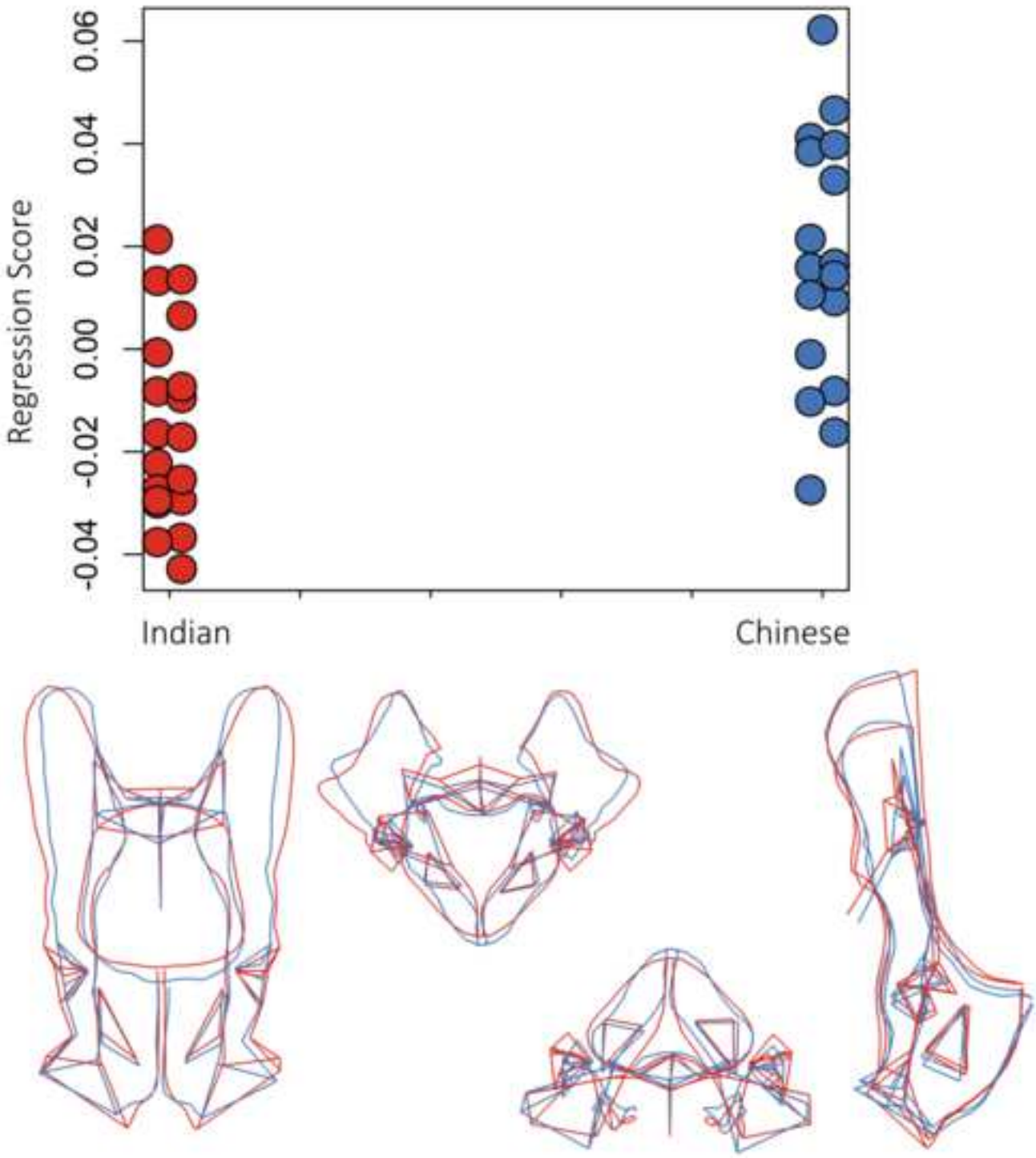

Figure 6

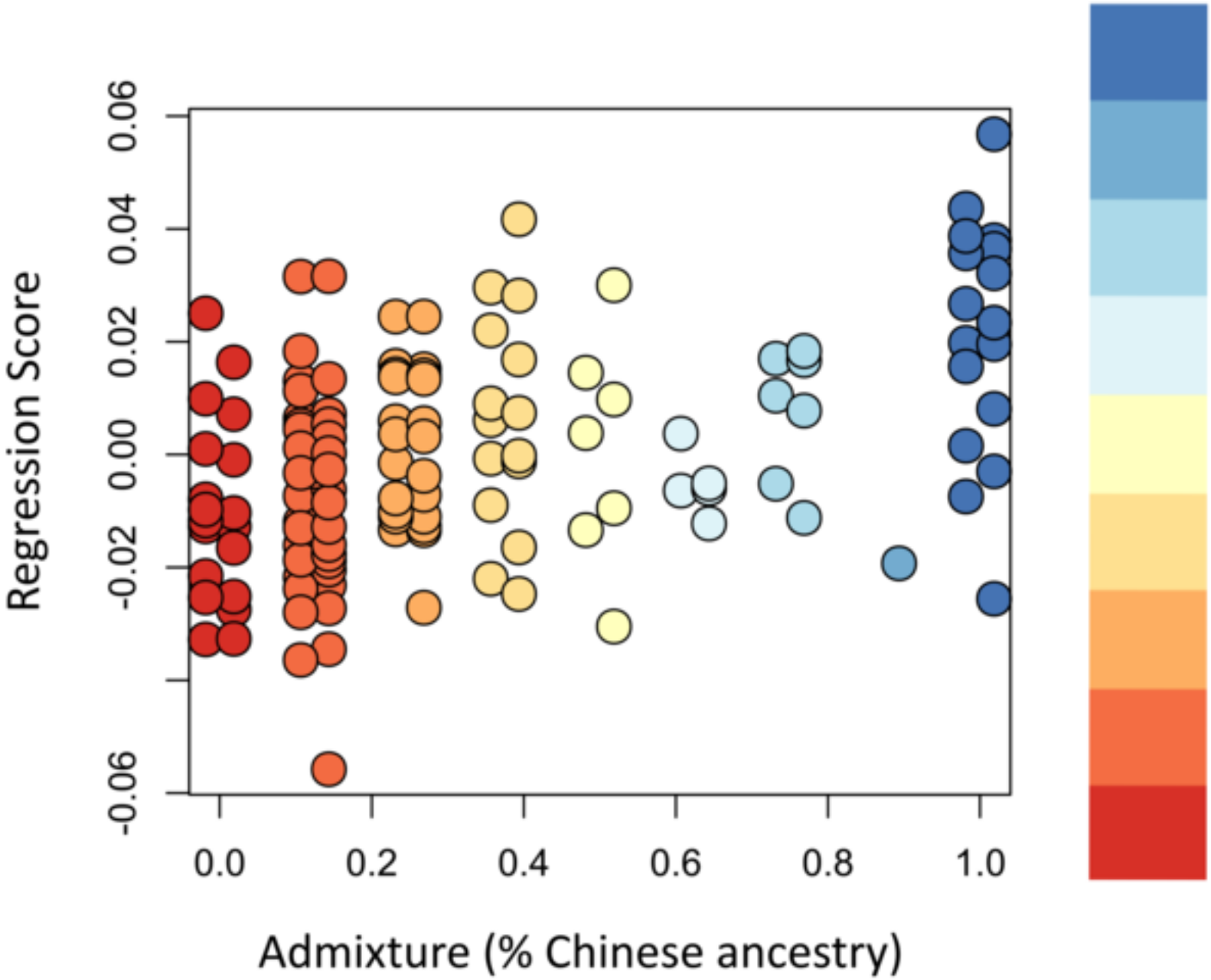
Regression Score
0.06
0.04
0.02
0.00
-0.02
-0.06
0.0
0.2
0.4
0.6
0.8
1.0
Admixture (% Chinese ancestry)

Figure 7

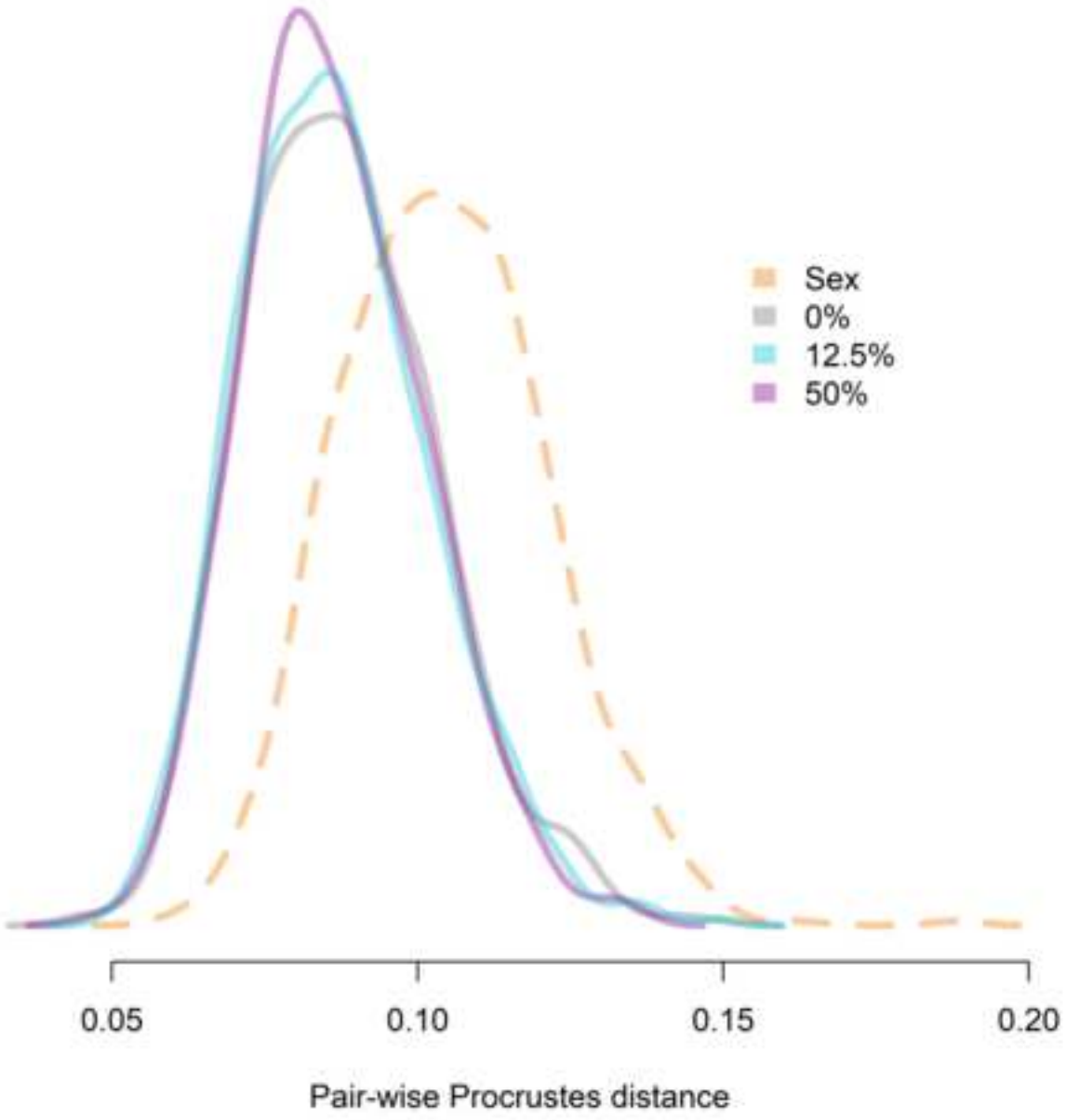

Table 1

Breakdown of sample (*n* = 138) by Chinese ancestry and sex. Ancestry category reflects the percentage of Chinese ancestry: 0% Chinese ancestry = full-bred Indian, 100% Chinese ancestry = full-bred Chinese. Full-bred sample *n* = 36.

Ancestry category	0%	12.5%	25%	37.5%	50%	62.5%	75%	87.5%	100%
Female	11	29	15	12	5	3	7	1	11
Male	8	15	8	3	2	2	0	0	6
Total	19	44	23	15	7	5	7	1	17

Table 2

Numbers and definitions of all landmarks (1 to 48) and semilandmarks (49 to 204).

Landmark number	Definition
1	Most cranial point on sacral wing—Right
2	Most caudoventral point on sacral wing, on linea terminali—Right
3	Most lateral point on cranial articular surface of S1—Right
4	Most ventral point on cranial articular surface of S1 body—Midline
5	Most ventral point on dorsal margin of articular cranial surface of S1 body—Midline
6	Most ventral point on cranial articular surface of S2 body—Midline
7	Most caudal point on sacrum—Midline
8	Dorsal caudal iliac spine—Right
9	Cranialmost point on iliac spine—Right
10	Cranialmost point on acetabular rim—Right
11	Medialmost point on cranial portion of lunate—Right
12	Medialmost point on caudal portion of lunate—Right
13	Centre of acetabulum—Right
14	Caudalmost point on acetabular rim—Right
15	Dorsalmost point on acetabular rim—Right
16	Ventrolateral point on lateral ischial crest at min. breadth—Right
17	Iliac blade medial (most medial intersection of iliac blade and sacrum)—Right
18	Dorsalmost point on ischial spine—Right
19	Intersection of dorsal ischial crest and ischial tuberosity—Right
20	Dorsalmost point on ischial tuberosity—Right
21	Most ventrolateral point on ischial tuberosity—Right
22	Most ventromedial point on ischial tuberosity—Right
23	Cranialmost point on obturator foramen—Right
24	Ventralmost point on obturator foramen—Right
25	Caudalmost point on obturator foramen—Right
26	Pubic symphysis cranial—Right
27	Most cranial point on sacral wing—Left
28	Most caudoventral point on sacral wing, on linea terminalis—Left
29	Most lateral point on cranial articular surface of S1—Left
30	Dorsal caudal iliac spine—Left
31	Cranialmost point on iliac spine—Left
32	Cranialmost point on acetabular rim—Left
33	Medialmost point on cranial portion of lunate—Left
34	Medialmost point on caudal portion of lunate—Left
35	Centre of acetabulum—Left
36	Caudalmost point on acetabular rim—Left
37	Dorsalmost point on acetabular rim—Left
38	Ventrolateral point on lateral ischial crest at min. breadth—Left
39	Iliac crest medial (most medial intersection of iliac crest and sacrum)—Left
40	Dorsalmost point on ischial spine—Left
41	Intersection of dorsal ischial crest and ischial tuberosity—Left
42	Dorsalmost point on ischial tuberosity—Left
43	Most ventrolateral point on ischial tuberosity—Left

44	Most ventromedial point on ischial tuberosity—Left
45	Cranialmost point on obturator foramen—Left
46	Ventralmost point on obturator foramen—Left
47	Most caudodorsal point on obturator foramen—Left
48	Pubic symphysis cranial—Left

Semilandmark number	Definition
49 to 88	Pelvic inlet curve
89 to 106	Dorsal ischial curve—Right
107 to 124	Dorsal ischial curve—Left
125 to 154	Iliac blade curve—Right
155 to 184	Iliac blade curve—Left
185 to 194	Pubic symphysis curve—Right
195 to 204	Pubic symphysis curve—Left

Table 3

Comparison (analysis of variance) of interactive and additive models for the relationship between sex, admixture (percent Chinese ancestry), and shape in the complete sample (*n* = 138). The larger interactive model is not a significantly better fit than the smaller additive model.

	Residual df	df	RSS	SS	r^2	F	*p*
Shape ~ sex + admix	135	1	0.508		0.000		
Shape ~ sex * admix	134	1	0.504	0.004	0.007	1.105	0.292
Total	137		0.635				

Table 4

Model comparison (analysis of variance) of three knot B spline and simple additive models for the relationship between shape and admixture in the complete sample (sex held constant for both variables). The B-spline model is not a significantly better fit than the smaller additive model.

	Residual df	df	RSS	SS	r^2	F	*p*
Additive	135	1	0.508		0.000		
B spline	130	5	0.489	0.120	0.307	1.038	0.388
Total	137		0.635				

Table 5

Analysis of variance of differences in centroid size between full-bred and admixed animals in the complete sample (*n* = 138).

	df	SS	MS	r^2	F	*p*
Admixture status[a]	2	11377	5688.70	0.04	2.58	0.07[b]
Residuals	135	298013	2207.50	0.96		
Total	137	309391				

[a]Admixture status groups: full-bred Indian, full-bred Chinese, admixed.

[b]There is no significant difference ($p > 0.05$) in centroid size between groups with different admixture status.

Table 6

Procrustes variances for admixture categories in the complete sample (*n* = 138).

Admixture status	Procrustes variance
Ind	0.0043
Chi	0.0049
Ad	0.0046

Abbreviations: Ind = full-bred Indian; Chi = full-bred Chinese; Ad = admixed.

Table 7

Test for significant differences in variance (Table 6) between full-bred and admixed animals in the complete sample (*n* = 138). Above the trace: pairwise differences between Procrustes variances; below the trace: *p*-values of tests of significance of differences.

	Ind	Chi	Ad
Ind	–	0.00054	0.00026
Chi	0.34	–	0.00028
Ad	0.53	0.54	–

Abbreviations: Ind = full-bred Indian; Chi = full-bred Chinese; Ad = admixed.

Table 8

Comparison (analysis of variance) of additive and interactive models of the relationship between sex, subspecies designation (Indian or Chinese), and shape in the full-bred sample (*n* = 36). The interactive model is a significantly better fit than the smaller additive model, as denoted by the significant (< 0.05) *p*-value.

	Residual Df	RSS	SS	R^2	F	*p*
Shape ~ sex + subspecies	33	0.149		0.000		
Shape ~ sex * subspecies	32	0.140	0.010	0.059	2.187	0.03
Total	35	0.160				